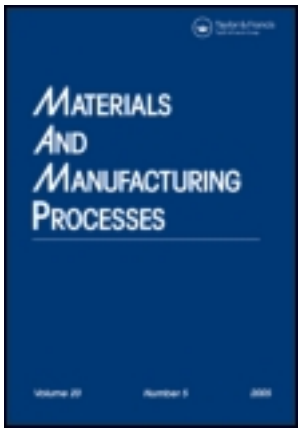

Materials and Manufacturing Processes
Publication details, including instructions for authors and subscription information:
http://www.tandfonline.com/loi/lmmp20

The Influence of Aluminum Content of AZ61 and AZ80 Magnesium Alloys on Hot Cracking

C. J. Huang [a] , C. M. Cheng [b] & C. P. Chou [a]
[a] Mechanical Engineering Department , National Chiao Tung University , Hsinchu, Taiwan
[b] Industrial Education , National Taiwan Normal University , Taipei, Taiwan
Accepted author version posted online: 24 May 2011.Published online: 19 Apr 2011.

To cite this article: C. J. Huang , C. M. Cheng & C. P. Chou (2011) The Influence of Aluminum Content of AZ61 and AZ80 Magnesium Alloys on Hot Cracking, Materials and Manufacturing Processes, 26:9, 1179-1187, DOI: 10.1080/10426914.2010.536936

To link to this article: http://dx.doi.org/10.1080/10426914.2010.536936

Materials and Manufacturing Processes, 26: 1179–1187, 2011

ISSN: 1042-6914 print/1532-2475 online
DOI: 10.1080/10426914.2010.536936

Taylor & Francis
Taylor & Francis Group

The Influence of Aluminum Content of AZ61 and AZ80 Magnesium Alloys on Hot Cracking

C. J. Huang[1], C. M. Cheng[2], and C. P. Chou[1]

[1]*Mechanical Engineering Department, National Chiao Tung University, Hsinchu, Taiwan*
[2]*Industrial Education, National Taiwan Normal University, Taipei, Taiwan*

This study aims to investigate how aluminum content in magnesium alloys AZ61 and AZ80 impacts the hot cracking susceptibility of magnesium alloys. Differences in aluminum content are known to influence the total crack length of hot cracking. Magnesium alloy AZ61's total crack length was the longest in one thermal cycle, while AZ80's total crack length increased as the number of thermal cycles increased. The most significant difference between AZ61 and AZ80 was the hot crack at the heat-affected zone (HAZ). As the number of heat inputs increased, the grain would coarsen in the HAZ and precipitation started, which resulted in the accumulation of hot cracks at weld metal HAZ (W. M. HAZ).

During the solidification of AZ80, which has higher aluminum content, the segregation of aluminum at the grain boundary caused $Mg_{17}Al_{12}$ to liquefy, increasing the length of hot cracks. Augmented strain caused miniature cracks between $Mg_{17}Al_{12}$ and grains. Therefore, aluminum content and augmented strain were found causes of hot cracking susceptibility in magnesium alloys.

Keywords AZ61; AZ80; Cracking; GTAW; $Mg_{17}Al_{12}$.

Introduction

Magnesium has excellent electromagnetic interference shielding properties, superior machinability, low densities, good thermal conductivity, strong shock absorption, and recyclable properties. It is widely used in many industries, such as automobile, aircraft, and electronic products [1–3]. Since welding technologies play an important role in joining applications. Laser beam welding (LBW), gas tungsten arc welding (GTAW), electron beam welding (EBW), and friction stir welding (FSW) [4–12] have been used in welding magnesium alloys. The most common defects of magnesium alloys during welding are: weakening at the heat-affected zone (HAZ) [13], hot cracking, distortion, and porosity [14]. They could weaken the joint after welding. Hot cracking is related to the composition of alloy itself and is closely associated with the contractions caused by regional heating and cooling during welding [15, 16].

Research of magnesium alloy's hot cracking susceptibility has not been published in present literature. Previous studies did not take multiple thermal cycles before welding into consideration when discussing the mechanical properties and microstructure of weld metal and HAZ. In the current study, we employed multiple thermal cycles to investigate how differences in thermal cycles and augmented strains affect aluminum content in AZ61 and AZ80, which leads to hot cracking and other results.

Received September 27, 2010; Accepted October 30, 2010

Address correspondence to C. J. Huang, Mechanical Engineering Department, National Chiao Tung University, Hsinchu, Taiwan; E-mail: sunstar123t@yahoo.com.tw

Experimental procedures

The materials used in the present study included hot-rolled plates of AZ61 and AZ80 magnesium alloys. The dimensions of each specimen were 200 mm × 35 mm × 3 mm. Table 1 shows the chemical compositions of AZ61 and AZ80.

This experiment used semi-automatic GTAW as a welding method to perform the single pass (one thermal cycle) and triple passes (triple thermal cycles) of specimens without filler materials using a W-ThO_2 electrode of 2.4 mm in diameter. Following experimental welding tests and corrections, the optimal welding parameters were discovered. Table 2 shows the relevant welding parameters.

Spot Varestraint Test

The hot cracking test involved a spot Varestraint test, which was carried out using the GTAW method. The instrument used in this test was a multiple Varestraint test instrument developed by the authors. The gun of the GTAW was controlled using a computer program to move along the *x* and *y* axes; die-blocks with various radii were set on the *x* or *y* axis. The stroke was adjustable to bend the materials to obtain the radius of the blocks. The block was changeable and the longitudinal Varestraint test was performed by setting the stroke using a single mechanism. Therefore, this instrument used for the spot Varestraint test, the longitudinal Varestraint test, and the Varestraint test of *x* and *y* axis welding was a multiple hot cracking test instrument.

Performing spot-welding on prewelded specimens enabled spot Varestraint tests, which involved spot welding of nonpass (nonthermal cycles), single pass (one thermal cycle), and triple pass (three thermal cycles) specimens (welding diagrams are shown in Fig. 1); 1%, 3%, and 5% augmented strains were applied. Table 3 shows the

TABLE 1.—Chemical composition of magnesium alloys, wt%.

	Element						
	Al	Zn	Mn	Si	Cu	Fe	Mg
AZ61	6.63	1.01	0.24	0.027	0.0026	0.0039	Bal.
AZ80	8.12	0.3	0.35	0.021	0.0023	0.0032	Bal.

TABLE 2.—Parameters for GTAW.

Current (A)	Voltage (V)	Travel speed (mm/min)	Argon flow rate (L/min)
100	10	60	10

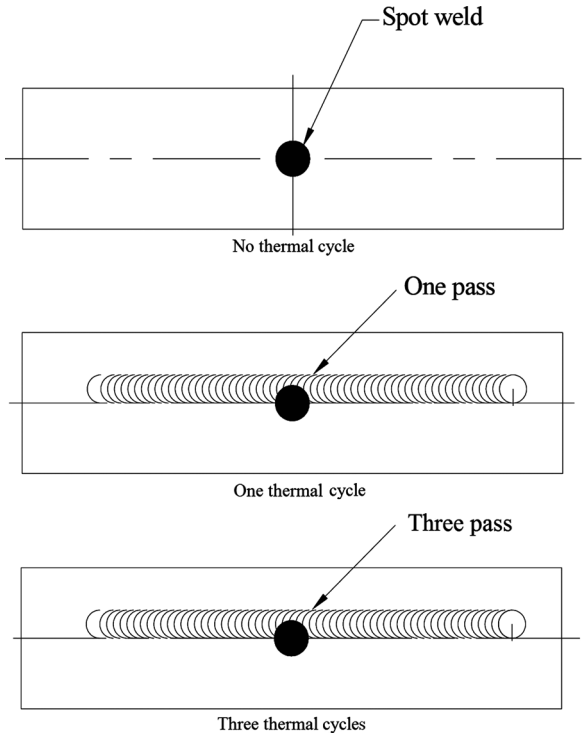

FIGURE 1.—Welding diagram.

spot Varestraint parameters. Following the tests, scanning electron microscope (SEM) was used to examine hot cracking in the fusion zone (FZ) and HAZ of specimens. The lengths of hot cracking specimens under different augmented strains and thermal cycles were analyzed to examine hot cracking susceptibility. The total crack length [17] for each specimen served as an indicator for hot cracking susceptibility. Etchant was produced by mixing

TABLE 3.—Parameters for spot Varestraint test.

Current (A)	Welding time (sec)	Argon flow rate (L/min)	Augment strain (%)
100	3	10	1, 3, 5

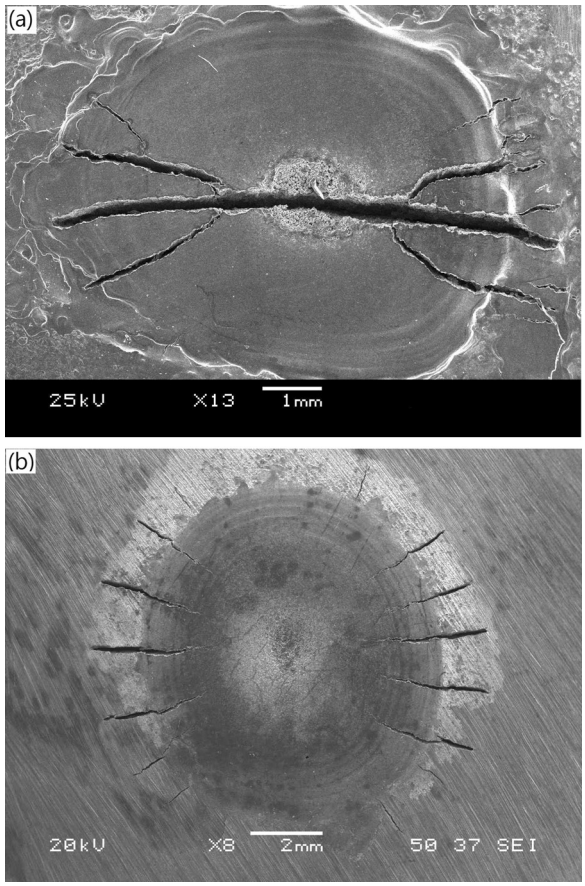

FIGURE 2.—Hot cracking in fusion zone of (a) AZ61 and (b) AZ80 (no thermal cycle).

4.2 g of picric acid +10 ml acetic acid +10 ml water and 70 ml ethyl alcohol for AZ61 and AZ80 [8], and was used to etch cross-sections of the specimen.

EXPERIMENTAL RESULTS AND DISCUSSION

SEM Observation

Figure 2 shows the SEM results of AZ61 and AZ80 under the varestraint test with no thermal cycle. As seen in the figure, while AZ61 did not undergo thermal cycle, hot cracking concentrated in the FZ. In contrast no cracks were found in HAZ. Hot cracks of AZ80 appeared in both FZ and HAZ with cracks extending from one to the other, possibly due to the increase of aluminum from 6% to 8%. Figure 3 shows the SEM picture of AZ61 during one thermal cycle and three thermal cycles. Hot cracks appeared in HAZ after one thermal cycle, but after three thermal cycles, a portion of cracks appeared in FZ, while most hot cracks were concentrated in the HAZ. Figure 4 shows the SEM picture of AZ80 after multithermal cycles; the location of hot cracks was similar to the one with no thermal cycle. It shows that AZ61's and AZ80's hot cracking susceptibility increased after multiple thermal cycles. Figure 5 shows the HAZ total cracking length measurements of AZ61 and AZ80 magnesium alloys under different augmented strains and different thermal cycles. Figure 5(a) shows that AZ61's total

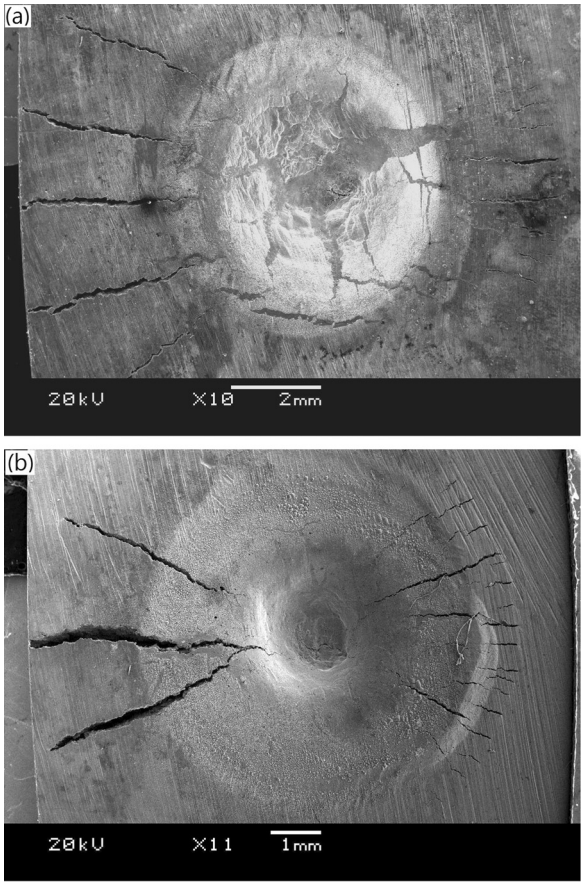

FIGURE 3.—Hot cracking in fusion zone and HAZ of AZ61 after (a) one thermal cycle and (b) three thermal cycles.

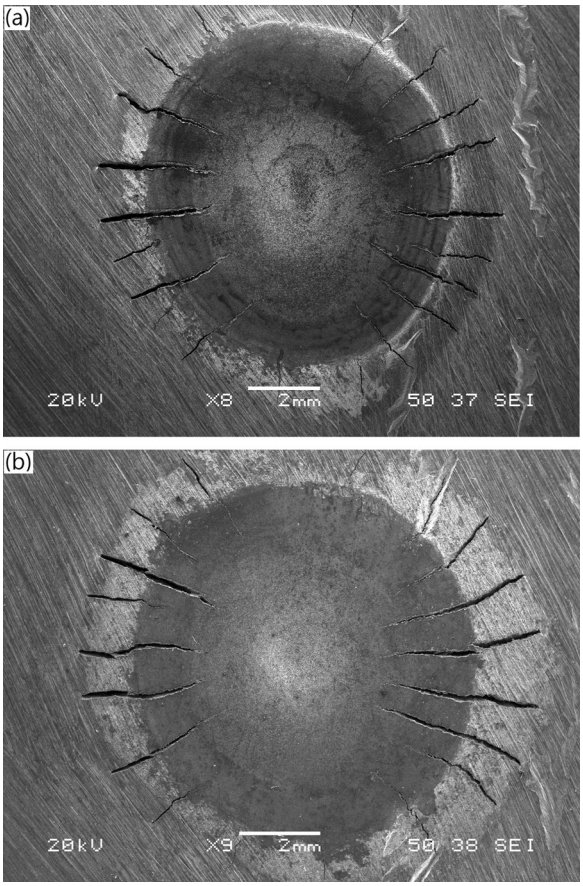

FIGURE 4.—Hot cracking in fusion zone and HAZ of AZ80 after (a) one thermal cycle and (b) three thermal cycles.

cracking length at one thermal cycle was longer than that at three thermal cycles. This result contradicts the hot cracking theories which posit that, under normal circumstances, the segregated elements in grain boundary increase as thermal cycles increase [18]. Figure 5(b) shows AZ80's HAZ total cracking length was longer at three thermal cycles than that at one thermal cycle, while the total crack length increased as thermal cycles accumulated.

Based on the location of HAZ, it can be classified as either base metal HAZ (B. M. HAZ) or weld metal HAZ (W. M. HAZ), as shown in Fig. 6. Our experimental results showed the hot cracking of AZ61 and AZ80's HAZ were mainly located at W. M. HAZ, while the length of hot cracking at B. M. HAZ were significantly shorter, as shown in Fig. 7.

To examine this phenomenon, hot crack lengths were collected from W. M. HAZ's and B. M. HAZ's of AZ61 and AZ80, respectively, with results shown in Fig. 8. Most HAZ's cracks were concentrated at W. M. HAZ, with only a small portion appearing at B. M. HAZ. Figure 8(a) shows that the total crack length of W. M. HAZ after three thermal cycles was shorter than one thermal cycle, which was not the case for B. M. HAZ. Figure 8(b) shows that the AZ80's HAZ cracks were spread evenly between W. M. HAZ and B. M. HAZ, and the total crack length of W. M. HAZ increased as the number of thermal cycles increased. This was likely caused by a lack of thermal refining after prewelding before undergoing Varestraint tests. As a result, weld metal became W. M. HAZ after heat was applied again. Grain coarsening and precipitation segregated in grain boundary both appeared in this region.

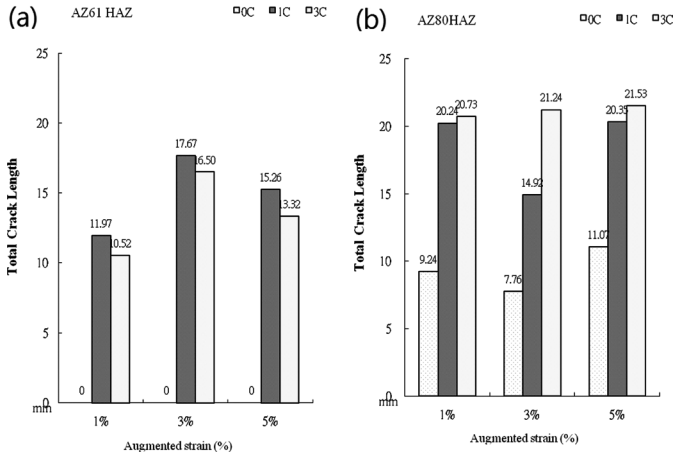

FIGURE 5.—Effect of number of thermal cycles on hot cracking in HAZ: (a) AZ61 and (b) AZ80.

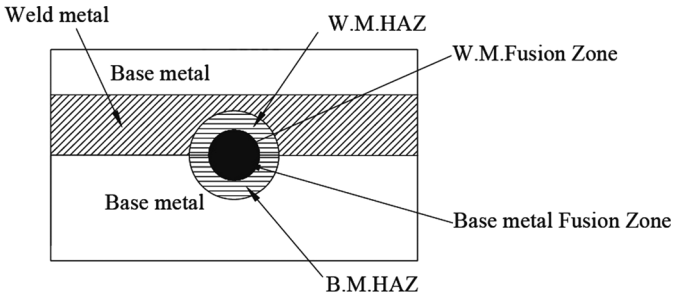

FIGURE 6.—Schematic drawing of W.M. HAZ and B.M. HAZ.

The differences in HAZ cracking length can be explained by the Mg-Al binary phase diagram. Figure 9 shows that AZ61's and AZ80's solidus and liquidus temperature range depends on Al content. This temperature range is called the partially melted zone (PMZ), which is wider for AZ80 and AZ61 that have higher Al content. Therefore, during Varestraint welding, the HAZ becomes a solid–liquid coexistence region with α Mg and liquid Mg. Being pulled by the augmented strain, the unsolidified liquid Mg were pulled apart before hot cracks appear in HAZ. Due to higher Al content in AZ61 and AZ80, liquid alloys with low melting point of liquid Mg were easily formed to yield wider PMZ. Liquid alloys stay within grain boundaries and create wider liquefied regions, resulting in longer hot cracks. Therefore, AZ61 and AZ80 have higher hot-cracking susceptibility in the W. M. HAZ.

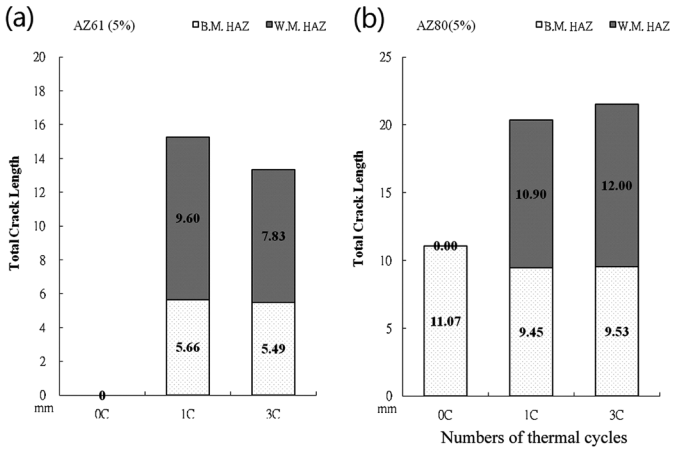

FIGURE 8.—Effects of number of thermal cycles on HAZ hot cracking with augment strain in (a) AZ61 and (b) AZ80.

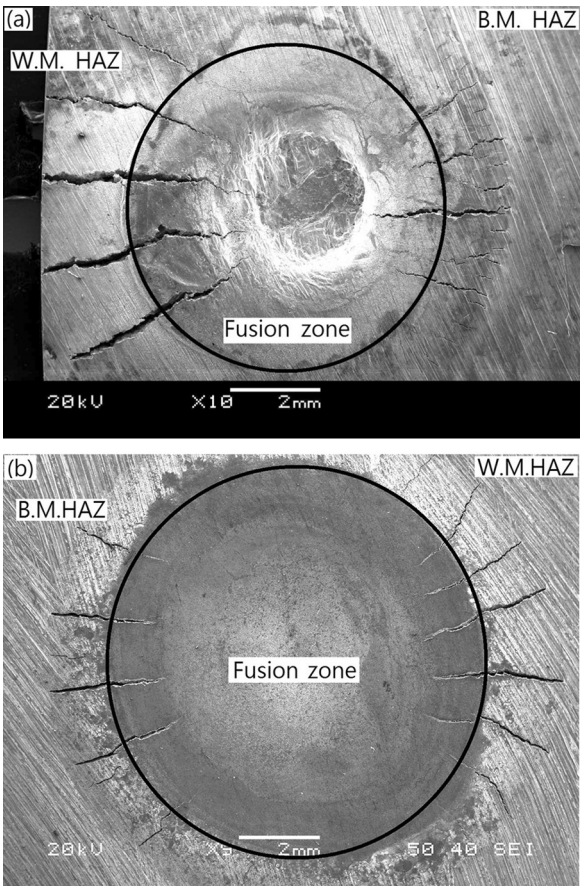

FIGURE 7.—Location of hot cracks in (a) AZ61 and (b) AZ80.

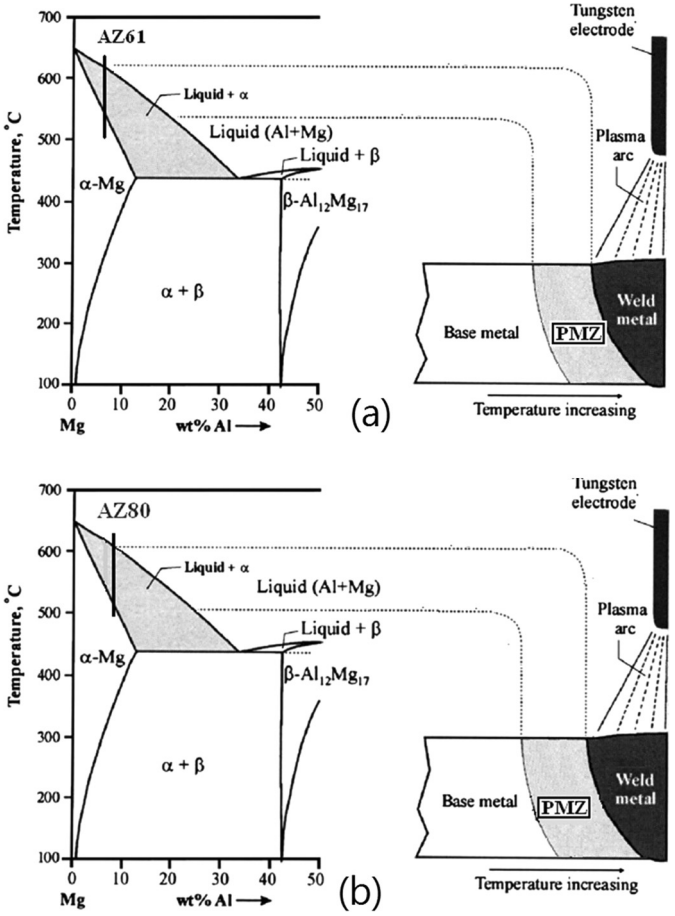

FIGURE 9.—Mg-Al binary phase diagram and schematic drawing of PMZ of arc weld in (a) AZ61 and (b) AZ80.

Hot Cracking Observation

Specimens of AZ61 and AZ80 were taken from the hot cracking cross-sections of B. M. HAZ and W. M. HAZ. The specimens were polished and etched before being placed under SEM. Figure 10 shows the AZ61 hot cracking cross-section after three thermal cycles. Precipitation was clearly visible between hot cracks and grains. Figure 10(a) shows a crack and a line of white precipitation. The precipitation around the edges of the cracks indicated the liquid alloy film had not solidified. This liquid alloy film was under augmented strain and later formed hot cracks during solidification. This corresponds to the mechanism of hot crack formation asserted by Borland [19]. The white precipitation around the grain boundary should be $Mg_{17}Al_{12}$, which showed no clear cracks at low magnification. The possible cause was most tension was located to the left of the crack, so the rest of the tension being unable to pull the liquid alloy film on the right; hence, the liquid alloy film became precipitation ($Mg_{17}Al_{12}$) during the cooling process. The precipitation ($Mg_{17}Al_{12}$) was magnified to 5,000 times in Fig. 10(b), and small cracks between precipitation and grains were visible, which indicates clear signs of tension that was not strong enough to separate the grains.

There were signs of $Mg_{17}Al_{12}$ around the grain boundary alongside AZ80's B. M. HAZ cracks [Fig. 11(a)]. Smaller cracks only appeared between $Mg_{17}Al_{12}$ and α Mg [Fig. 11(b)]. In other words, if liquefied $Mg_{17}Al_{12}$ was not present within the grain boundary during the final solidification process, hot cracks could not be formed. This proves that low melting point $Mg_{17}Al_{12}$ around the grain boundary was one of the causes for hot cracking in magnesium alloys.

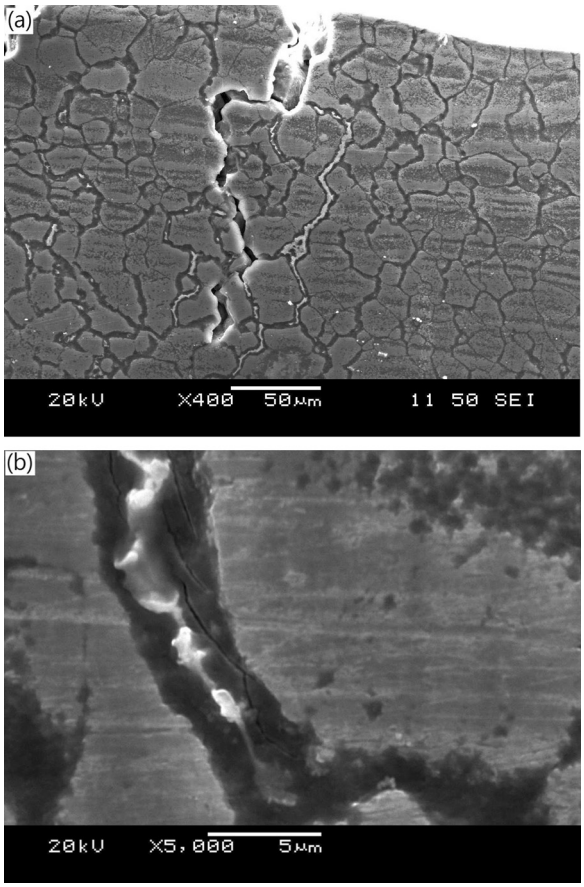

FIGURE 10.—(a) AZ61 hot cracks and precipitation with (b) detail showing small hot cracks around precipitation.

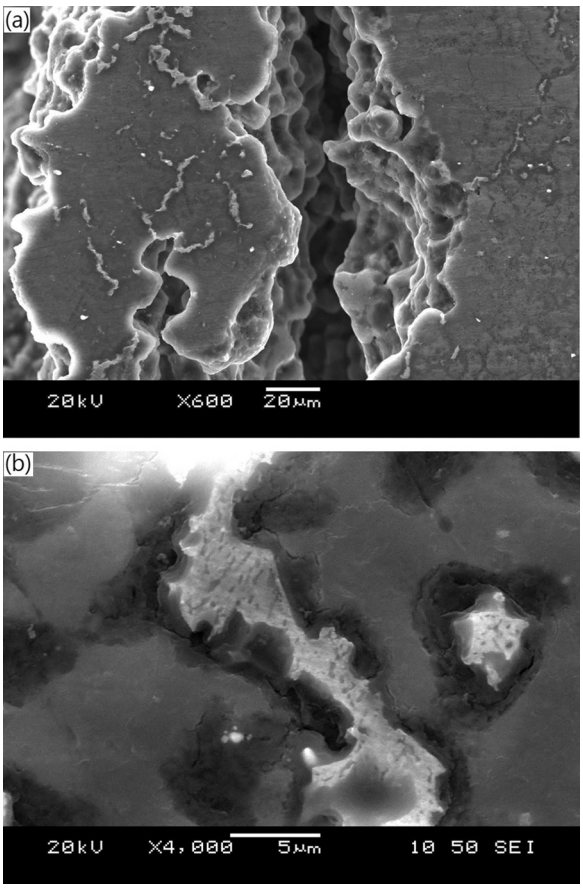

FIGURE 11.—(a) AZ80 hot cracks and precipitation with (b) detail showing small hot cracks around precipitation.

Energy Dispersive Spectrometer (EDS) Analysis

Grain Boundary Analysis of W. M. HAZ. This experiment used AZ61 and AZ80 specimens that had been through one thermal cycle and three thermal cycles, and then performed EDS analysis on the grains near the W. M. HAZ cracks, as shown in Fig. 12. The AB line could be divided into five equal parts, 3-µm long each, and it was the scanning path across the grain boundary.

Figure 13(a) shows the results of scanning through Al of the AB line. Results showed segregation of Al around the grain boundary (beside the cracks) of AZ61. At one thermal cycle, Al content at the grain boundary was 15.66 wt%, much higher than the original of 6.0 wt%. At three thermal cycles, it dropped to 10 wt%, which was only 4 wt% higher than base metal. It could be deduced that as more heat was delivered in three thermal cycles, a portion of Al evaporated, causing the Al content to drop. The melting

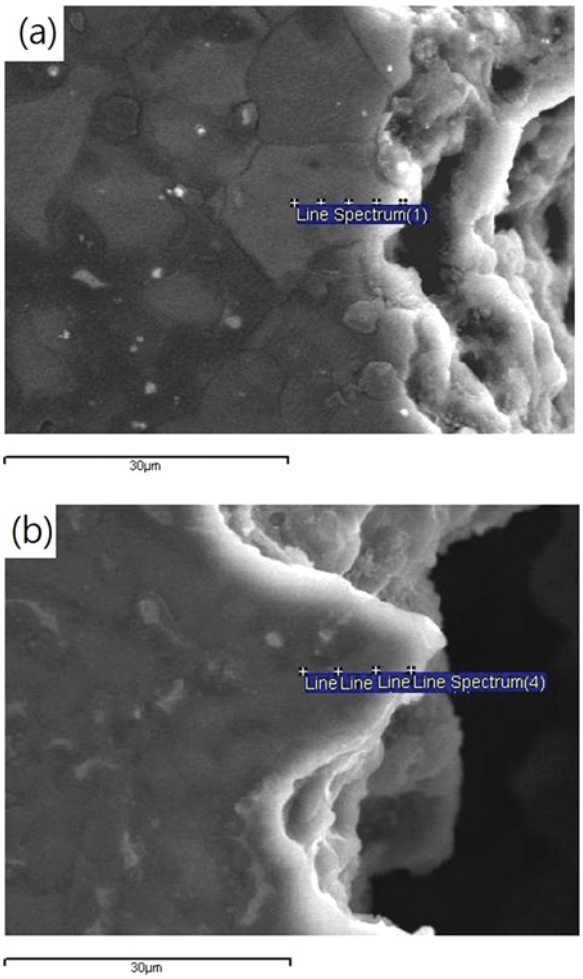

FIGURE 12.—EDS analyses of grain boundary of (a) AZ61 and (b) AZ80 (color figure available online).

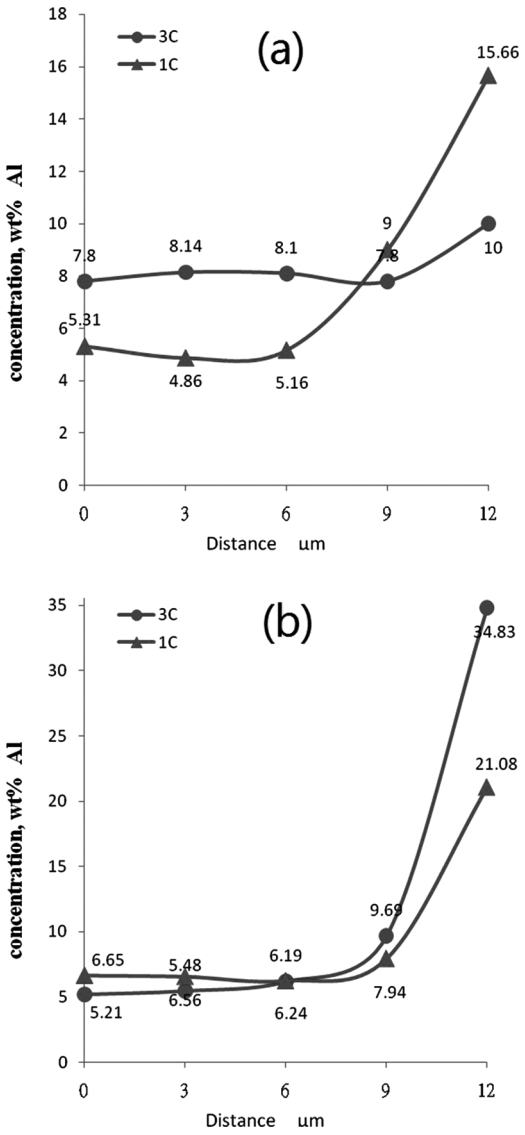

FIGURE 13.—EDS analysis data of grain boundary of (a) AZ61 and (b) AZ80.

point and boiling point of Al are 600°C/2060°C [20], while the temperature of a created electric arc could be beyond 8000°C [21], which explains the evaporation of Al after multiple welding processes. As the Al content dropped in the liquid alloy at three thermal cycles, its melting point was higher, and hence, the shorter total hot cracking length than with that at one thermal cycle. To prove the reduction in Al content, specimens of AZ61 W. M. HAZ were taken after one thermal cycle and three thermal cycles. Figure 14 shows the analyses of W. M. HAZ and the hot cracking surface. Results are shown in Table 4. Specimens from one thermal cycle and three thermal cycles both contained 6.9 wt% of Al, 0.7 wt% of Zn, both similar to contents in the AZ61. This could mean the alloy element contents within W. M. HAZ were unchanged. Analyses of crack surfaces showed Al content of 11 wt% for one thermal cycle, while the Al content was 8 wt% for three thermal cycles, a significant reduction in Al.

Specimens of AZ80 after three thermal cycles showed Al content at 34.83 wt% around the grain boundary, four times as high as the base metal 8.0 wt%, while the Al content was 21.08 wt% in one thermal cycle [Fig. 13(b)]. Previous studies [15, 16] showed that the segregation of alloy elements increases as the number of thermal cycles increases. The total crack length of three thermal cycles was significantly longer than in the case of one thermal cycle, which suggests Al segregation as a cause for hot cracking. Therefore, the amount of Al could be used to access magnesium alloy's hot-cracking susceptibility. However, AZ80's Al segregation at three thermal cycles did not reduce the Al content. This was probably due to the fact that higher Al content in AZ80 would evaporate without affecting Al precipitation on the hot crack surfaces, even though the remaining Al still created a large amount of $Mg_{17}Al_{12}$. Figure 15 shows the sphere $Mg_{17}Al_{12}$ spreads in W. M. HAZ of AZ61; $Mg_{17}Al_{12}$ of AZ80 spreads evenly within the grain boundary. After multithermal cycles, the web $Mg_{17}Al_{12}$ remelting could create belt shape $Mg_{17}Al_{12}$, forming the hot cracks more easily.

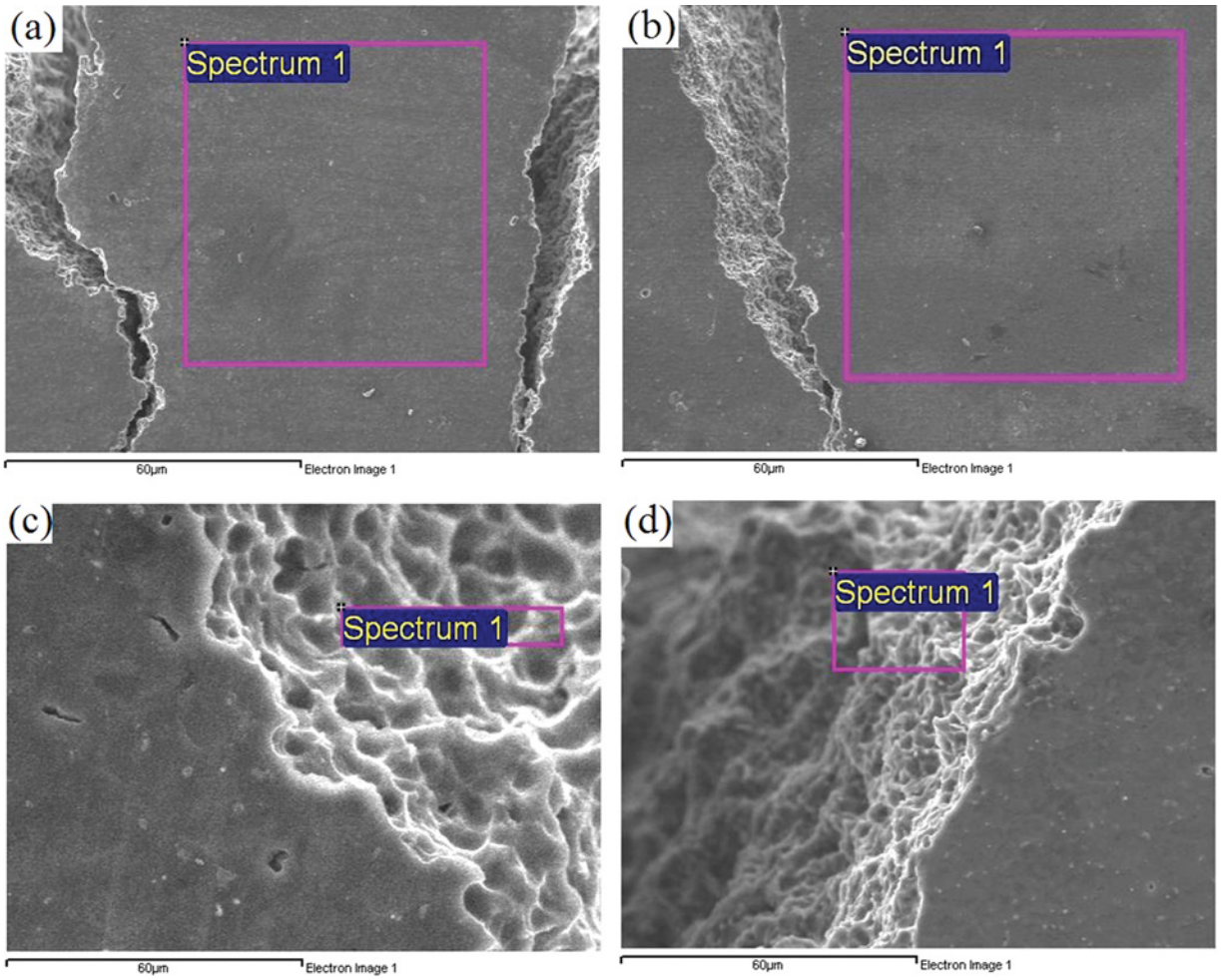

FIGURE 14.—Location of AZ61 for EDS analyses: (a) 1 thermal cycle W.M. HAZ, (b) 3 thermal cycle W.M. HAZ, (c) 1 thermal cycle hot cracking surface, (d) 3 thermal cycle hot cracking surface (color figure available online).

TABLE 4.—EDS results of Fig. 14 alloy contents (wt%).

	Element		
	Al	Zn	Mg
1C-W. M. HAZ	6.92	0.71	Bal.
3C-W. M. HAZ	6.94	0.64	Bal.
1C-hot cracking surface	11.06	1.49	Bal.
3C-hot cracking surface	8.7	0.71	Bal.

To prove that the precipitation within the grain boundary was $Mg_{17}Al_{12}$, specimens of AZ61 M. W. HAZ were analyzed with EDS, as shown in Fig. 16. The results are in Table 5. The results of the analysis showed that the precipitation was indeed $Mg_{17}Al_{12}$. Yakubtsov [22] investigated AZ80 magnesium alloy at different thermal processes by heating AZ80 followed by natural cooling. The resultant $Mg_{17}Al_{12}$ precipitation within the grain boundary is shown in Fig. 17. No obvious signs of cracks in the picture indicated that no hot cracks existed between $Mg_{17}Al_{12}$ and α Mg, showing that no augmented strain was present. Hence, the miniature cracks created in this experiment were caused by augmented strains.

CONCLUSIONS

The proposed experiment put AZ61 and AZ80 magnesium alloys through multi-thermal cycles and augmented strain via Varestraint tests. Accordingly, the following conclusions were reached based on analyses of SEM and EDS results.

The Al content of AZ61 and AZ80 can be used to assess the hot-cracking susceptibility, because the more the Al content is, the more precipitation ($Mg_{17}Al_{12}$) with low melting point is produced at grain boundaries. This is verifiable given the type of $Mg_{17}Al_{12}$, because point $Mg_{17}Al_{12}$ scattered over the W. M. HAZ of AZ61; nevertheless, web $Mg_{17}Al_{12}$ scattered over the W. M. HAZ of AZ80. So AZ80 has more $Mg_{17}Al_{12}$ than AZ61. During welding process, $Mg_{17}Al_{12}$ will melt in grain boundaries and cause liquefaction, and at the same time, augmented strain pulls away the grain boundaries, forming the hot cracking. AZ80 is more prone to form hot cracking.

In three thermal cycles AZ61's Al content was lower than one thermal cycle from EDS results. This is attributable

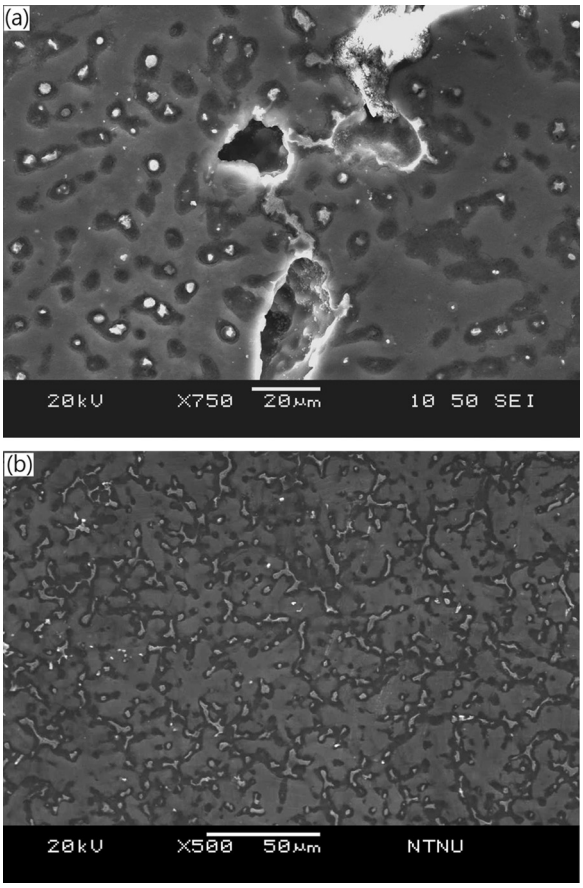

FIGURE 15.—The spread of $Mg_{17}Al_{12}$ at W.M. HAZ in (a) AZ61 and (b) AZ80.

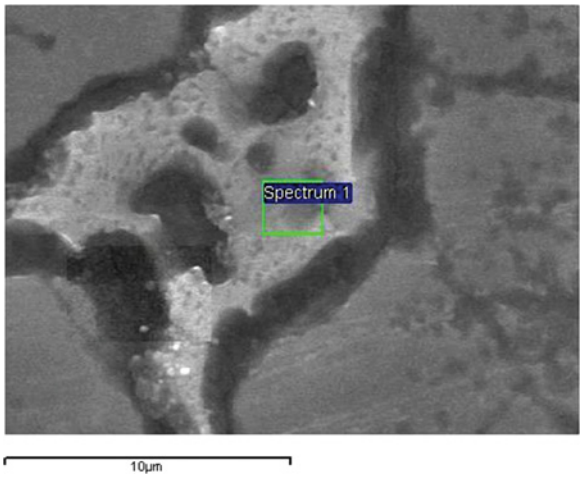

FIGURE 16.—EDS analysis of $Mg_{17}Al_{12}$ (color figure available online).

TABLE 5.—EDS results of Fig. 16 alloy contents (wt%).

	Element		
Precipitation	Al	Zn	Mg
$Mg_{17}Al_{12}$	35.69	1.43	Bal.

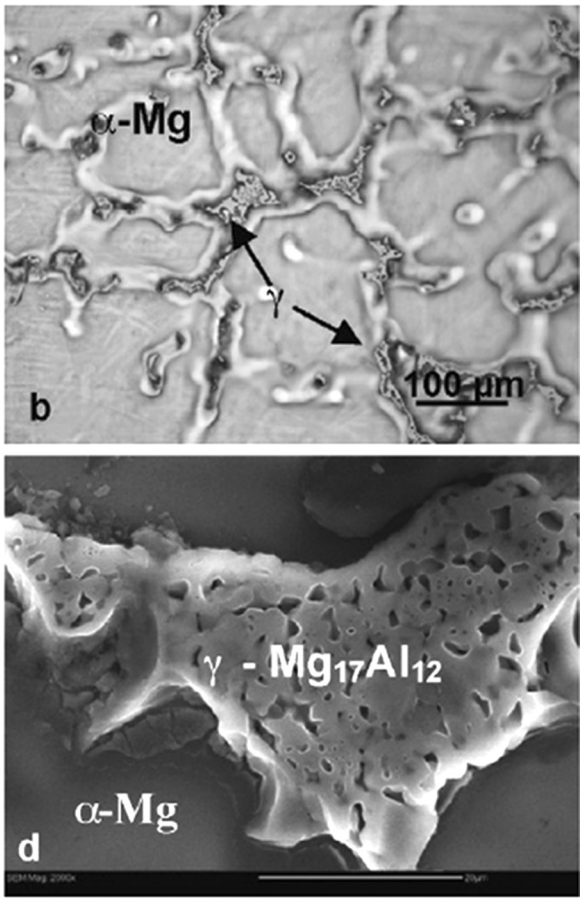

FIGURE 17.—$Mg_{17}Al_{12}$ and α magnesium [21].

to the evaporation of Al due to the number of heat input, resulting in less Al in the liquid alloy film (having a higher melting point). Thus, the region of grain liquefaction was smaller than one thermal cycle. AZ80's hot cracks existed in FZ and HAZ in all specimens. AZ80 has higher Al content and will cause more $Mg_{17}Al_{12}$ at the grain boundaries of HAZ. During heat input, $Mg_{17}Al_{12}$ will liquefy at grain boundaries and cause the grain liquefaction of a broad region. Therefore, AZ80 has higher hot cracking susceptibility.

Spot varestraint tests can be used to find serviceable material for repair welding or multiwelding for thick plates. Our findings suggest that AZ61can be welded for repair welding (or thick plate welding), whereas AZ80 cannot be welded for repair welding.

REFERENCES

1. Kulekci, M.K. Magnesium and its alloys applications in automotive industry. International Journal of Advanced Manufacturing Technology **2008**, *39*, 851–65.
2. Mordike, B.L.; Ebert, T. Magnesium: Properties-applications-potential. Material Science and Engineering A **2000**, *302*, 37–45.
3. Cao, X.; Xiao, M.; Jahazi, M.; Immarigeon, J.P. Continuous wave Nd:YAG laser welding of sand-cast ZE41A-T5 magnesium alloys. Journal of Materials and Manufacturing Processes **2005**, *20*, 987–1004.

4. Manti, R.; Dwivedi, D.K. Microstructure of Al-Mg-Si weld joints produced by pulse TIG welding. Journal of Materials and Manufacturing Processes **2007**, *22*, 57–61.
5. Park, S.H.C.; Sato, Y.S.; Kokawa, H. Effect of micro-texture on fracture location in friction stir weld of Mg alloy AZ61 during tensile test. Scripta Materialia **2003**, *49*, 161–166.
6. Lee, W.B.; Yeon, Y.M.; Jung, S.B. Joint properties of friction stir welded AZ31B-H24 magnesium alloy. Journal of Materials Science and Technology **2003**, *19*, 785–790.
7. Mclean, A.A.; Powell, G.L.F.; Brown, I.H.; Linton, V.M. Friction stir welding of magnesium alloy AZ31B to aluminium alloy 5083. Science and Technology of Welding and Joining **2003**, *8*, 462–464.
8. Hu, L.J.; Peng, Y.H.; Li, D.Y.; Zhang S.R. Influence of dynamic recrystallization on tensile properties of AZ31B magnesium alloy sheet. Journal of Materials and Manufacturing Processes **2010**, *25*, 880–887.
9. Coelho, R.S.; Kostka, A.; Pinto, H.; Riekehr, S.; Kocak, M.; Pyzalla, A.R. Microstructure and mechanical properties of magnesium alloy AZ31B laser beam welds. Material Science and Engineering A **2008**, *485*, 20–30.
10. Su, S.F.; Huang, J.C.; Lin, H.K.; Ho N.J. Electron beam welding behavior in Mg-Al based alloys. Material Science and Engineering A **2002**, *33*, 1461–1473.
11. Liu, L.M.; Shen, Y.; Zhang, Z.D. The effect of cadmium chloride flux in GTA welding of magnesium alloys. Science and Technology of Welding and Joining **2009**, *11*, 398–402.
12. Commin, L.; Dumont, M.; Masse, J.E.; Barrallier, L. Friction stir welding of AZ31 magnesium alloy rolled sheets: Influence of processing parameters. Acta Materialia **2009**, *57*, 326–334.
13. Baeslack, W.A.; Savage, S.J.; Froes, F.H. Laser-weld heat-affected zone liquation and cracking in a high strength Mg-based alloy. Material Science Letters **1986**, *6*, 935–939.
14. Shen, J.; You, G.Q.; Long, S.Y.; Pan, F.S. Abnormal macropore formation during double-sided gas tungsten arc welding of magnesium AZ91D alloy. Materials Characterization **2008**, *59*, 1059–1065.
15. Cheng, C.M.; Chou, C.P.; Lee, I.K.; Lin, H.Y.. Hot cracking of welds on heat treatable aluminium alloys. Science and Technology of Welding and Joining **2005**, *10*, 344–352.
16. Huang, C.; Kou, S. Partially melted zone in aluminum welds: Solute segregation and mechanical behavior. Welding Journal **2001**, *1*, 9–17.
17. Bollinghaus, T. *Hot Cracking Phenomena in Welds II*; Springer-Verlag: Berlin, 2008.
18. Sindo K. *Welding Metallurgy*; Wiley: New York, 2003.
19. Borland, J.C. Generalized theory of super-solidus cracking in welds (and castings). British Welding Journal **1960**, *7*, 508–512.
20. Leong, K.H.; Kornecki, G.; Standers, P.G.; Keske, J.S. Laser beam welding of AZ31B-H24 alloy. In *17th International Congress on Applications of Lasers and Electro-Optics (ICALEO '98)*, Orlando, FL, November 16–19, 1998; 28–36.
21. Ribic, B.; Palmer, T.A.; DebRoy, T. Problems and issues in laser-arc hybrid welding. International Materials Reviews **2009**, *54*, 223–244.
22. Yakubtsova, I.A.; Diaka, B.J.; Sagera, C.A.; Bhattacharyab, B.; MacDonald, W.D.; Niewczasb, M. Effects of heat treatment on microstructure and tensile deformation of Mg AZ80 alloy at room temperature. Material Science and Engineering A **2008**, *496*, 247–255.